batteries

MDPI

Review

Focused Ion Beam-Defined Analytical Geometries for Correlative Battery Characterization

Jiaqi Jia [1,*], Yong Li [1], Ke Deng [1], Yuchen Li [1], Zhao Ding [1] and Maziar Ashuri [2,*]

[1] College of Materials Science and Engineering, Chongqing University, Chongqing 400044, China
[2] Department of Mechanical, Materials, and Aerospace Engineering, Illinois Institute of Technology, Chicago, IL 60616, USA
* Correspondence: cq-jiaqi@cqu.edu.cn (J.J.); mashuri@hawk.iit.edu (M.A.)

Abstract

Battery reactions and degradation processes frequently originate or evolve at buried interfaces, extend through complex three-dimensional composite architectures, and change with electrochemical state. Analysis of an exposed surface or an arbitrarily selected cross-section can therefore lose the positional, volumetric, or state information required for interpretation. This focused Review organizes FIB-supported correlative battery characterization according to three analytical dimensions established by focused ion beam (FIB)-defined geometries: position, depth/volume, and electrochemical state/time. Four representative workflows—orientation-preserving lift-out, tomography-guided exposure, serial PFIB-EDS-SIMS sectioning, and FIB-prepared operando observation windows—are examined through a common measurement-to-claim chain comprising geometry definition, direct signal acquisition, data transformation, derived quantities, and the highest physical inference supported by the evidence. The comparison identifies workflow-specific uncertainties associated with target relocation, milling depth, matrix effects, slice spacing, cross-modal registration, segmentation, and observation-window perturbation. It further distinguishes local structural or chemical association, cross-depth persistence, and state-resolved morphology from stronger claims concerning transport, kinetics, or degradation mechanisms, which require independent electrochemical, mechanical, spectroscopic, or modelling evidence. This framework provides a basis for selecting FIB-defined analytical geometries, reporting their uncertainty, and matching the resulting evidence to defensible physical claims in battery characterization.

Keywords: focused ion beam; battery microscopy; correlative microscopy; FIB-SIMS; plasma FIB; three-dimensional elemental reconstruction; operando FIB-SEM

Check for updates

Academic Editor: Nikhil A. Koratkar

Received: 12 August 2026
Revised: 27 August 2026
Accepted: 1 September 2026
Published: 3 September 2026

Copyright: © 2026 by the authors. Licensee MDPI, Basel, Switzerland. This article is an open access article distributed under the terms and conditions of the Creative Commons Attribution (CC BY) license.

1. Introduction

Battery electrodes operate through ionic, electronic, chemical, and mechanical processes that are distributed across heterogeneous microstructures and coupled over several length scales. Because these processes are spatially heterogeneous and state-dependent, both location and history determine how an observation should be interpreted. Reaction state may vary from the current-collector side to the electrolyte-facing side of a porous coating; buried pores, inclusions, and cracks may affect only a subset of particles; and contact loss can appear during delithiation, partly close during lithiation, or remain after discharge [1–5]. These phenomena lead to three experimental questions: where the observed signal or feature is located within the original electrode architecture, how far the

associated structure extends beyond a single plane, and at what electrochemical state the feature forms or changes. High spatial resolution alone cannot answer these questions if positional, volumetric, or state information has been lost during specimen preparation or analysis.

Conventional characterization methods leave different parts of this problem unresolved. SEM resolves exposed morphology, but the meaning of a cross-section depends on where that plane was created. X-ray tomography locates internal structures and bridges particle, electrode, and device scales, yet light-element chemistry and fine interphases may remain unresolved [6–9]. EDS provides robust contrast for many non-Li elements, while SIMS offers Li- and isotope-sensitive signals only after a surface has been exposed; those signals also depend on matrix composition, sputtering, charging, and topography [10–12]. Post-mortem imaging preserves a final state but usually not the order or reversibility of the events that produced it. The analytical gap is therefore not a simple lack of resolution. It is the absence of a controlled relation between the detector signal and the original position, depth/volume, or electrochemical state of the material.

FIB can restore this missing analytical relation by controlling where material is removed and which geometrical context is retained. During lift-out, milling can preserve a device-referenced position while converting a porous electrode into an analytically accessible specimen; after tomography, it can expose a feature that was localized within a preceding volume; in serial sectioning, it defines the depth order of successive analytical planes; and in operando experiments, it enables repeated access to the same cross-section at defined electrochemical states. A conventional cross-section remains sufficient when local morphology alone answers the scientific question. FIB becomes measurement-defining when the interpretation depends on retained position, depth order, or repeated access to the same region during electrochemical evolution.

Previous FIB-SIMS reviews have primarily emphasized instrumentation, secondary-ion signal formation, analytical capabilities, and method-specific limitations [11,12], whereas recent battery-focused FIB-SEM reviews have provided broad surveys of specimen preparation, three-dimensional reconstruction, multimodal correlation, chemical analysis, and operando applications [13]. The present Review adopts a different organizing principle. Rather than classifying techniques, it asks when the geometry created by FIB becomes part of the measurement itself and what level of physical claim that geometry can support. This distinction leads to the analytical-dimension framework and the measurement-to-claim chain used throughout this Review. Complementary guidelines for reactive alkali-metal systems show that storage, inert transfer, ion-source selection, temperature, and beam dose can determine whether a targeted region preserves its native structure and chemistry [14].

Four representative workflows are selected because together they isolate the three analytical dimensions considered in this Review. Orientation-preserving lift-out and tomography-guided exposure both establish positional information, but they do so from different prior knowledge: the former retains a device-referenced electrode direction, whereas the latter relocates a feature identified within a preceding three-dimensional dataset [15,16]. Serial Xe-PFIB sectioning adds controlled depth order and supports reconstruction of elemental persistence and adjacency across multiple planes [17]. An FIB-prepared operando observation window instead preserves access to the same local cross-section at defined electrochemical states, thereby adding state/time information to the structural observation [18]. These workflows are used as representative cases for a common methodological comparison rather than as an exhaustive survey of FIB applications.

Each workflow is evaluated through the same measurement-to-claim chain: (i) the FIB-defined analytical geometry, (ii) the directly acquired signal, (iii) registration, resampling, segmentation, reconstruction, or other data transformation where applicable, (iv) the

resulting derived quantity or descriptor, and (v) the highest physical claim supported by that evidence. This framework separates measurements from reconstructions and interpretations and makes explicit where uncertainty enters the evidence chain. Relocation error, matrix effects, milling-depth uncertainty, slice-spacing variation, registration residuals, segmentation sensitivity, beam-induced modification, and limited sampling are considered only insofar as they affect the validity of the final claim. The resulting comparison is intended to provide a practical basis for workflow selection and evidence reporting rather than another catalogue of FIB capabilities.

2. When FIB Defines the Measurement

FIB may expose, extract, serially section, or refresh the face of a battery specimen. In the workflows considered here, the operation becomes measurement-defining when moving the final plane or changing the access geometry would alter the scientific comparison. Shifting a lift-out along the electrode thickness changes the positional meaning of the SIMS map; changing serial slice spacing changes the reconstructed adjacency of elemental domains; and altering the operando window changes both the region and the mechanical boundary followed during cycling. The relevant object is therefore the FIB-defined analytical geometry to which the detector signal is assigned.

2.1. Analytical Dimensions Established by FIB-Defined Geometries

Figure 1 summarizes the three FIB-defined geometries using a common sequence from analytical geometry to directly acquired information and the resulting analytical output. A targeted surface preserves positional information by assigning SEM or chemical-mapping signals to a defined analytical plane, thereby enabling position-resolved local chemical analysis. Serial PFIB sectioning establishes depth/volume information by generating a controlled sequence of surfaces whose elemental maps can be registered to evaluate three-dimensional elemental persistence and adjacency. An FIB-prepared observation window retains electrochemical state/time information by enabling the same local cross-section to be revisited at selected stages of cycling, thereby resolving state-dependent local structural evolution [15–18].

These geometries are not arranged as a hierarchy of increasing sophistication. Each resolves a different missing analytical dimension. A targeted plane is sufficient when the question concerns where a local chemical or structural signal is located; serial sectioning is required when the claim depends on persistence or adjacency beyond one plane; and a revisited observation window is required when the onset or partial reversibility of a structural event is unresolved. Additional acquisition is justified only when it removes an ambiguity relevant to the scientific claim, because each added dimension also introduces additional registration, preparation, sampling, or perturbation requirements.

2.2. From Acquired Signal to Defensible Claim

A defensible interpretation requires a distinction among the signal that is acquired, the transformations subsequently applied to that signal, and the physical claim derived from the processed data. In this Review, each workflow is therefore described using five linked levels: FIB-defined geometry → directly acquired signal → data transformation → derived quantity or descriptor → supported physical claim. SEM, EDS, and SIMS images are directly acquired signals; co-registered volumes, segmented phase domains, and geodesic-distance distributions are generated only after additional processing. The evidential strength of the final claim depends on whether the uncertainties introduced at each intermediate step are small enough relative to the spatial or temporal relation being interpreted.

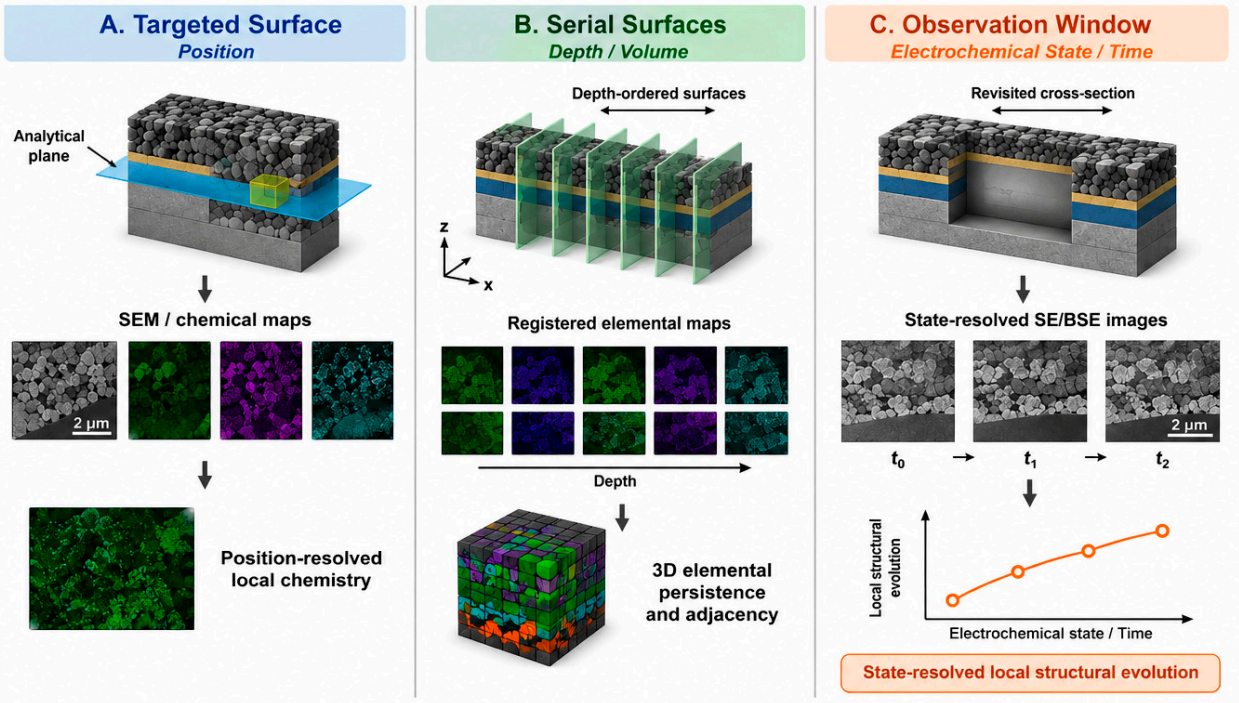


Figure 1. Schematic illustration of FIB-defined analytical geometries and the analytical dimensions they preserve or establish in correlative battery characterization. (**A**) A targeted surface assigns SEM or chemical-mapping signals to a defined analytical plane, thereby preserving positional information and enabling position-resolved local chemical analysis. (**B**) Serial PFIB sectioning generates a depth-ordered sequence of analytical surfaces whose elemental maps can be registered to evaluate three-dimensional elemental persistence and adjacency within the analyzed volume. (**C**) An FIB-prepared observation window enables the same local cross-section to be revisited at selected electrochemical states, thereby providing state/time-resolved information on local structural evolution. The three geometries address different analytical ambiguities—position, depth/volume, and electrochemical state/time—and should be selected according to the information required for the final physical claim. Blue denotes the targeted analytical plane, green denotes the serial depth-ordered surfaces, and orange denotes electrochemical-state/time-resolved evolution; arrows indicate the progression from the FIB-defined geometry to the acquired or derived analytical information.

Apparent co-location depends on registration, three-dimensional distributions depend on resampling and stacking, and geometrical descriptors depend on segmentation and subsequent calculation. A registration offset can change whether a Li-sensitive domain is assigned to an active-material particle, a neighboring electrolyte, or an interfacial region; similarly, a change in segmentation threshold can alter whether a geometrical path remains connected. Claims of transport limitation, reaction heterogeneity, or degradation mechanism therefore require either demonstrated robustness to these analytical choices or independent electrochemical, mechanical, spectroscopic, or modelling support.

Local credibility and broader representativeness must be evaluated separately. For a local measurement, the target must be relocated accurately; milling, transfer, vacuum exposure, and beam dose must not generate the contrast being interpreted; cross-modal registration error must be smaller than the spatial relation being assigned; and an operando window must not dominate the fracture or contact change under study. Cryogenic transfer or milling can reduce reaction and redistribution in sensitive battery materials, but dose, temperature, and transfer history remain necessary [19,20]. Even when these conditions are met, one deliberately selected crack or particle does not establish electrode-wide prevalence; that requires repeated regions selected by a defined sampling strategy. These two questions—whether a local observation is analytically credible and whether it is representa-

tive of a broader electrode population—should therefore be reported separately throughout correlative FIB studies.

3. Targeted Surfaces for Position-Dependent and Buried Features

Local chemistry becomes difficult to interpret when the analytical surface has lost its relation to the electrode architecture. Through-thickness gradients require the collector-to-electrolyte direction to remain recoverable, whereas sparse buried defects require their coordinates to be known before destructive exposure. Targeted FIB preparation addresses both problems by placing one analytical plane according to a rule defined before the final measurement.

3.1. Through-Thickness Lift-Out

Composite electrodes can develop position-dependent reaction states, surface films, and access to ionic or electronic pathways. A particle near the current collector is not equivalent to one near the electrolyte-facing surface, even when their local morphologies appear similar. An unspecified cross-section may show composition or cracking, but it cannot assign the observation to electrode depth.

Delfino et al. [15] used an orientation-preserving lift-out workflow to extract and reorient a through-thickness electrode region while retaining its original collector-to-electrolyte direction and generating a sufficiently flat surface for SIMS analysis. The methodological value of this procedure is therefore not the lift-out operation itself, but the preservation of positional context during specimen transformation. Subsequent chemical signals can be assigned to electrode depth, a tracked particle, or a defined interface rather than to an otherwise positionless fragment. At the same time, flattening and final polishing reduce—but do not eliminate—topography-dependent SIMS artifacts.

Flatness matters because SIMS intensity is sensitive to local incidence angle, shadowing, extraction geometry, and sputter yield. A rough porous surface can generate apparent hotspots at particle edges or depressions even when the underlying concentration is unchanged. Calibration studies and battery applications show that matrix effects and edge effects remain central when Li-sensitive signals are compared across chemically dissimilar domains [10,21–23]. Ion polishing reduces topographic ambiguity, but it does not convert intensity into an absolute concentration or guarantee preservation of the native surface. Air exposure, vacuum residence, protective deposition, local heating, implantation, redeposition, and preferential sputtering may all modify mobile or reactive species. Cryogenic FIB and cryo-transfer can preserve lithium metal and solid–liquid interfaces more effectively, yet they still require documented dose, temperature, and transfer conditions [19,20,24,25]. A through-thickness trend therefore needs more than one well-prepared block: multiple regions selected by a stated rule are required before local positional differences can be generalized.

The same positional principle extends beyond the FIB-SIMS workflow illustrated in Figure 2. For example, site-specific FIB preparation has been used to prepare matched STEM and atom-probe specimens from defined depths of layered cathode secondary particles, allowing local Li concentration and structural evolution to remain associated with their original particle coordinate [26]. More broadly, correlative workflows can retain or recover a preselected battery region for higher-resolution downstream analysis [27], provided that the selection rule and specimen history remain traceable. For highly reactive battery materials, this requirement must be considered together with environmental and beam-induced alteration. Recent correlative-imaging guidelines for alkali-metal systems show that inert-gas transfer, ion-source selection, temperature, and electron/ion dose can determine whether the prepared region remains representative of the native material [14]. The

positional advantage of targeted preparation is therefore meaningful only when specimen preservation is demonstrated independently.

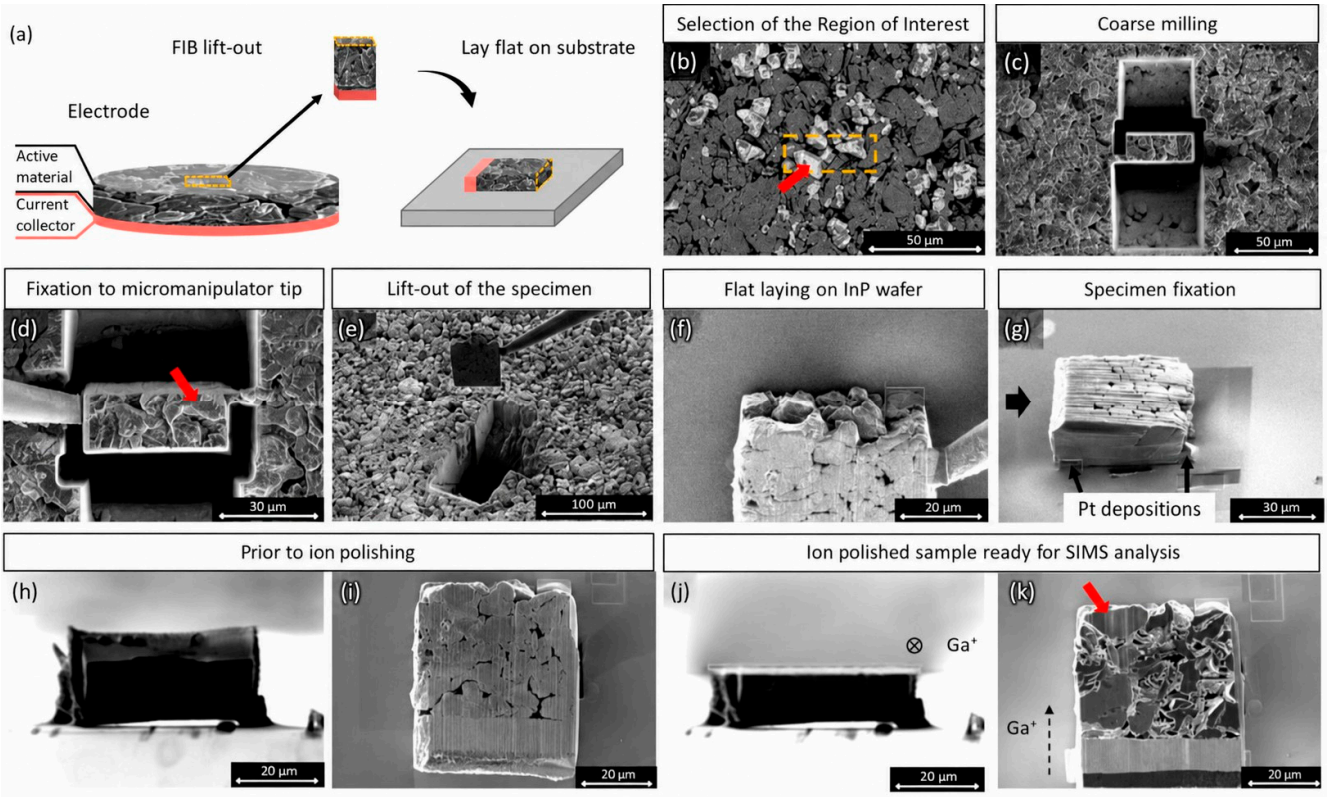


Figure 2. Orientation-preserving lift-out of a through-thickness analytical surface. (**a**) Schematic illustration of FIB lift-out positioning for subsequent SIMS analysis; (**b**) BSE image showing the selected region of interest (ROI), with the yellow dashed box defining the target region and the red arrow identifying a tracked Si–C composite particle; (**c**) coarse milling around the selected ROI; (**d**,**e**) attachment to the micromanipulator and extraction of the selected specimen; (**f**) placement of the specimen flat on an InP support; (**g**) fixation by ion-beam-induced Pt deposition; (**h**,**i**) specimen before ion polishing; and (**j**,**k**) ion-polished specimen ready for SIMS analysis. In panel (**b**), the brighter particles correspond to the Si–C composite and the darker particles to graphite; the red arrow tracks the same Si–C particle through the preparation sequence. Adapted with permission from Ref. [15].

3.2. Tomography-Guided Exposure

Cressa et al. [16] combined nanoCT-guided localization with FIB exposure and SIMS to examine intact and cracked regions within a mixed LCO/NCA cathode, as summarized in Figure 3. NanoCT first located the target features at a reported resolution of 224 ± 23 nm; FIB then exposed a plane approximately 1.5 µm below the pillar surface, after which SEM resolved local morphology and SIMS recorded relative $^{7}Li^{+}$, $^{27}Al^{+}$, and $^{59}Co^{+}$ signals. The essential analytical link is therefore not simply CT followed by SIMS, but relocation of the final chemical measurement to a feature identified in the preceding three-dimensional dataset.

Because FIB milling and SIMS sputtering are destructive, the defensible correlation is between the final analytical plane and the feature recorded before milling, rather than between two unchanged volumes. This distinction defines the evidentiary value of tomography-guided exposure: it allows local chemistry to be associated with a prelocated structural feature, but it does not establish whether the chemistry caused that feature or developed subsequently.

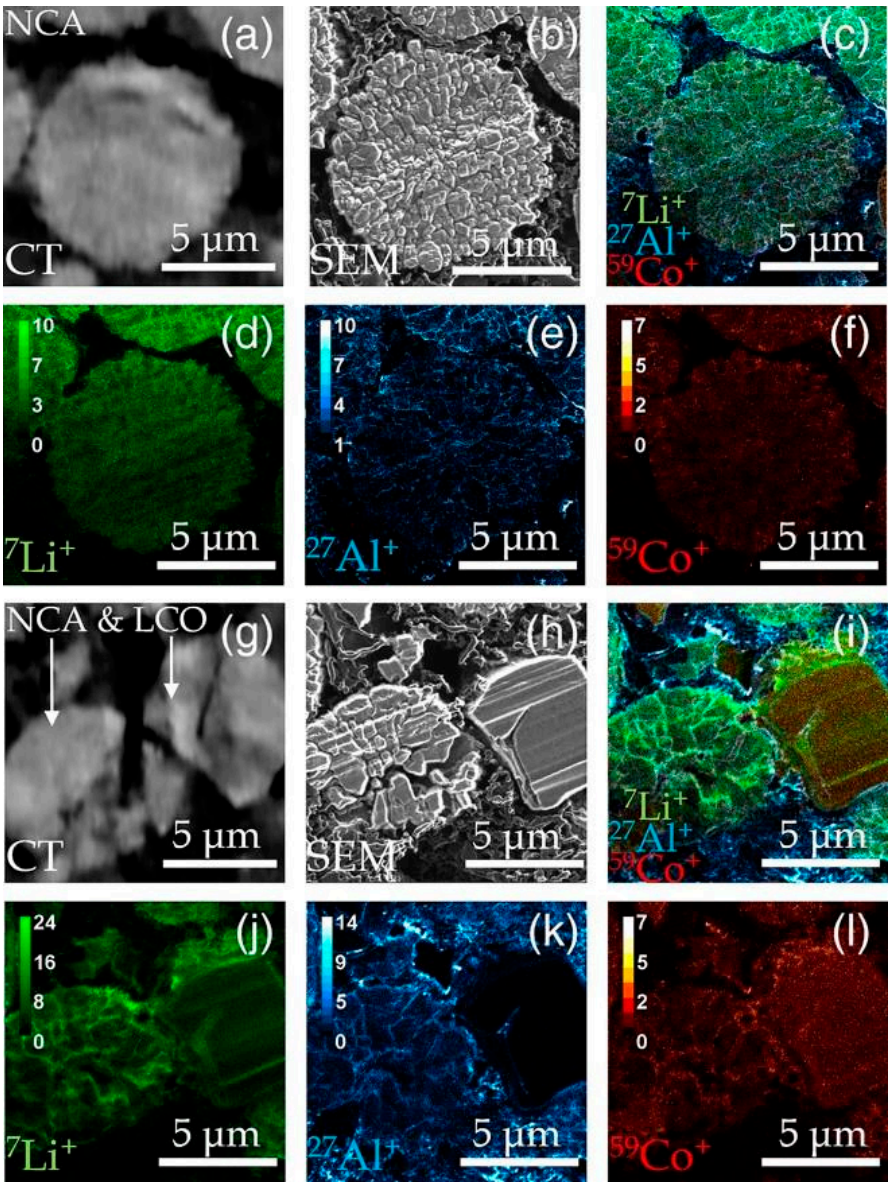


Figure 3. Tomography-guided exposure of prelocated cathode features. NanoCT, SEM, and SIMS data are correlated for an intact NCA particle (**a**–**f**) and an adjacent cracked NCA/LCO region (**g**–**l**) exposed by FIB at an approximate depth of 1.5 µm. The CT images identify the target before destructive sectioning, SEM resolves the exposed morphology, and SIMS provides relative $^{7}Li^{+}$, $^{27}Al^{+}$, and $^{59}Co^{+}$ signals. Intensity bars report detected secondary ions per pixel rather than calibrated concentrations. Scale bar: 5 µm. Adapted with permission from Ref. [16].

The strength of the inference depends on both signal physics and relocation accuracy. SIMS intensity remains relative unless matrix-matched calibration is available, and assignment to a specific feature depends on the combined uncertainty from CT resolution, stage relocation, milling depth, drift, and cross-modal alignment. A feature should be appreciably larger than that uncertainty before its chemistry is attributed to a particular crack or interface. Selecting an anomalous particle also introduces sampling bias; repeated features, control regions, multiple electrochemical states, or a larger-scale dataset are needed for causal or electrode-wide claims.

Taken together, orientation-preserving lift-out and tomography-guided exposure illustrate two forms of positional control [15,16]. The first preserves a coordinate that is known before specimen extraction, whereas the second recovers a coordinate that is identified within a preceding volume. Correlative X-ray/FIB tomography provides a related example

in which the same electrode location is interrogated across different spatial scales, allowing a larger-volume structural dataset to constrain the region selected for higher-resolution FIB analysis [8]. Related site-specific FIB workflows can extend the same principle to downstream TEM, STEM, atom-probe tomography, or chemically sensitive analysis, but the evidentiary requirement remains unchanged: the final analytical signal must remain traceable to the selection rule used before destructive preparation. In reactive battery systems, preservation studies further show that positional fidelity alone is insufficient if environmental exposure or ion-beam modification alters the material during transfer or milling [14]. Thus, target definition and specimen preservation should be treated as separate validation requirements.

4. Serial Surfaces for Three-Dimensional Elemental Reconstruction

A single cross-section can show that two phases meet on one plane, but it cannot determine whether the contact persists, terminates, or reconnects outside that plane. Serial sectioning converts this unknown out-of-plane extension into a measured depth sequence. The scientific question is therefore whether an element-associated domain or interface observed locally remains present across adjacent sections, not whether the final rendering appears visually three-dimensional.

4.1. Why a Single Cross-Section Is Insufficient

A single cross-section cannot establish whether an apparent phase contact, pore, crack, or conductive domain persists outside the plane. FIB-SEM reconstruction has consequently been used to quantify phase fractions, tortuosity, carbon-binder domains, and cycling-induced microstructural changes, while complementary tomography and multi-scale statistical methods can test whether a local reconstruction represents the surrounding electrode [9,28–36]. The methodological distinction is important: planar adjacency becomes a three-dimensional claim only when persistence and connectivity are examined across depth.

EDS and SIMS provide complementary contrast in heterogeneous battery electrodes: EDS robustly maps many heavier elements, whereas SIMS supplies a practical Li-sensitive channel when Li K X-ray mapping is inadequate [37]. Xe-PFIB can define a rapid depth sequence [38], but serial maps become interpretable only after their slice spacing, surface quality, drift, and cross-modal alignment are placed in a common coordinate system.

4.2. Co-Registration of EDS and SIMS Through Serial PFIB Sectioning

Sun et al. [17] constructed a serial PFIB–EDS–SIMS dataset comprising 39 depth-ordered planes spanning approximately 2.3 μm through an all-solid-state composite cathode. Each plane combines morphological information with heavier-element EDS channels and a Li-sensitive SIMS channel. Because the modalities differ in field of view, pixel size, interaction volume, and signal physics, the individual images do not constitute a three-dimensional dataset until normalization, resampling, and cross-modal registration are performed. The reported reconstruction used an $81.4 \times 81.4 \times 60$ nm^3 voxel grid, making registration and slice-spacing uncertainty directly relevant to any claim of interfacial adjacency.

Figure 4 displays the registered relative $^6Li^+$, Co, C, Al, and Zr signal domains within the reconstructed volume. Their cross-slice persistence and adjacency can be examined directly, but they are not exact phase boundaries because interaction volumes and ion yields blur nanoscale interfaces. Strong $^6Li^+$ variation within $LiCoO_2$ therefore supports local signal heterogeneity under the selected conditions; phase fraction, interface area, connectivity, and percolation require separate segmentation and sensitivity analysis.

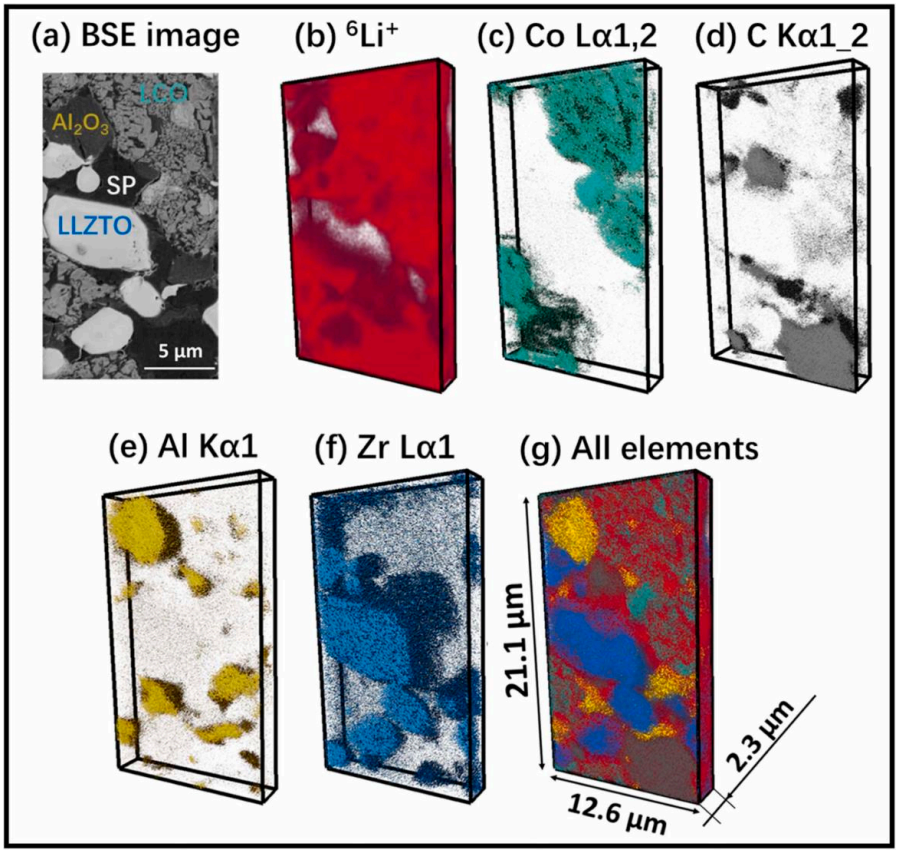


Figure 4. Serial Xe-PFIB sectioning and correlative elemental reconstruction of an all-solid-state composite cathode. Thirty-nine BSE/EDS/SIMS planes span approximately 2.3 µm. Relative Co, C, Al, Zr, and $^6Li^+$ maps were normalized, resampled, registered, and reconstructed at 81.4 × 81.4 × 60 nm^3 per voxel. The individual volumes show the spatial extent of phase-associated signals, and the combined rendering visualizes their adjacency within the analyzed region. Intensities are relative signal distributions, not calibrated elemental concentrations. In the rendered elemental maps, $^6Li^+$ is shown in red/magenta, Co in cyan/teal, C in grayscale, Al in yellow, and Zr in blue; the combined rendering overlays these elemental channels. Adapted from Ref. [17] under a Creative Commons Attribution 4.0 license.

4.3. What the Reconstruction Can—and Cannot—Support

The transformation from individual maps to a registered volume introduces the main uncertainty. Normalization changes contrast without identifying the physical source of intensity variation; resampling creates common coordinates without improving intrinsic resolution; and nominal voxel dimensions do not represent isotropic chemical resolution. Beam size, electron-interaction volume, sputter mixing, roughness, drift, and registration residuals must therefore be compared with the feature being interpreted. Alignment landmarks, residual error, excluded regions, and sensitivity to small translations or rotations should be reported. If an apparent interfacial enrichment disappears after a shift comparable to the registration error, the data support only a broader phase association.

Uncertainty also accumulates along the milling direction. Composition-dependent removal, redeposition, curtaining, missing slices, and stage error can alter the nominal increment, so total removed depth or an independent calibration is needed. EDS interaction volumes limit phase-boundary precision; carbon contrast may miss finely dispersed conductive additive, and an Al signal cannot resolve a nanoscale Al_2O_3 shell as a continuous coating. SIMS adds high Li sensitivity but retains matrix-dependent yield and possible beam-induced redistribution [11,12]. Under these constraints, the reconstruction supports relative elemental extension and adjacency within the analyzed volume; validated seg-

mentation may additionally support candidate connectivity. It does not measure Li flux, conductivity, reaction rate, or electrode-scale prevalence.

The reconstructed volume is also a selected sample of a heterogeneous electrode. A few hundred cubic micrometres can contain several particles and interfaces, yet it may still miss larger-scale gradients in compaction, carbon distribution, crack density, or electrolyte connectivity. A local volume is appropriate for resolving interfacial adjacency at the voxel scale; it is not, without repeated volumes or multiscale correlation, a basis for electrode-wide phase fractions. This distinction is especially important when image-based transport models are built from one reconstruction. Numerical precision in the model cannot compensate for an untested assumption that the imaged volume represents the electrode population. The reporting quantities required to test these limitations—slice-spacing variation, registration residual, excluded sections, and segmentation sensitivity—are summarized in Table 1.

Table 1. Measurement-to-claim framework, validation requirements, and claim limits for FIB-defined analytical geometries.

Workflow	Missing Analytical Dimension	Direct Evidence	Transformation/ Derived Quantity	Uncertainty and Minimum Validation to Report	Highest Defensible Claim
Orientation-preserving lift-out	Position within the electrode architecture	SEM or chemical-mapping signals from a plane with retained electrode orientation	Assignment of local signals to electrode depth, interface, or tracked particle	Orientation landmarks and retained electrode direction; transfer and milling history; final-polish conditions; beam energy/current or cumulative dose where relevant; estimated target-position/depth uncertainty; surface/topography check for SIMS; number of independently analyzed ROIs (n) when broader trends are claimed.	Local chemistry differs at a defined position within the electrode architecture.
Tomography-guided exposure	Position of a buried or prelocated feature	Local morphology or chemical signal acquired after targeted FIB exposure	Cross-modal registration of the final analytical plane to the pre-imaged feature	Tomographic voxel size and effective spatial resolution; target-localization uncertainty; stage-relocation error; nominal and verified milling depth; cross-modal registration residual (pixels and/or physical length); final-plane verification; number of target and control regions.	A defined buried feature is spatially associated with a measured local signal.
Serial PFIB-EDS-SIMS	Depth/volume	Depth-ordered BSE/EDS/SIMS maps from successive FIB-generated planes	Normalization, resampling, registration, segmentation where required, and three-dimensional stacking	Mean slice spacing and its variation; total calibrated removed depth; voxel dimensions; number of acquired and excluded/missing slices; registration residual for each modality or representative distribution; sensitivity of phase fraction/connectivity/adjacency to plausible segmentation thresholds; SIMS matrix-effect controls where required.	Relative elemental domains persist across specified depths and exhibit defined three-dimensional adjacency; connectivity requires validated segmentation.
FIB-prepared operando observation window	Electrochemical state/time	Repeated SE/BSE morphology of the same local cross-section at defined electrochemical states	Image registration, segmentation, and state-dependent geometrical descriptors where applicable	Cell/trench dimensions; applied stack pressure and comparison with the reference cell; OCV or resistance offset relative to an unmodified configuration; beam dose and cleaning history for each state; image-registration residual; segmentation sensitivity of derived descriptors; number of tracked particles/windows; explicit identification of measured and simulated states.	A local structural event occurs at a defined electrochemical state and partly recovers or persists under the reported observation-window conditions.

5. Operando Windows for Electrochemical Evolution

A final crack image contains no timestamp. It cannot distinguish a pre-existing defect from one opened during delithiation, partly closed during lithiation, or introduced during disassembly and post-mortem preparation. The same ambiguity applies to gaps at active-material/solid-electrolyte interfaces. An FIB-prepared window retains local cross-sectional access while electrochemical state changes, allowing event order and partial reversibility to be observed, but the window also becomes part of the mechanical and electrochemical experiment.

5.1. Resolving Electrochemical-State Ambiguity

In this Review, operando is reserved for measurements acquired while the cell remains under active electrochemical control and the analytical signal is temporally coupled to device operation. When the cell is first brought to a defined electrochemical state and the electrochemical drive is then paused or held while imaging is performed, the measurement is described as state-resolved in-cell (or quasi-operando where that terminology is used in the source study). Measurements performed after disassembly or removal from the operating cell are described as post-mortem. These categories should not be used interchangeably because they support different claims about event timing and transient behavior.

Perrenot et al. [18] used an FIB-prepared observation window to image the same local cross-section of an NMC622/Li_3PS_4 solid-state cell during galvanostatic cycling while electrical connection and mechanical loading were maintained. This operando geometry complements larger-field operando X-ray tomography [3–5,39,40] by testing whether a fine structural feature existed before cycling, formed during a defined electrochemical step, or partially recovered afterward.

Within the observed region, selected intraparticle gaps opened or widened during delithiation and narrowed during subsequent lithiation, while some NMC622/Li_3PS_4 separation persisted after discharge [18]. These observations establish event order and local partial reversibility; they do not directly measure resistance, current distribution, Li flux, or the cause of particle-to-particle variation.

Particle-to-particle variation remained substantial, and the image sequence could not separate the effects of orientation, constraint, contact area, and local reaction state. Its direct contribution is narrower: it distinguishes fractures opened during a defined electrochemical step from pre-existing or purely post-mortem defects and tests their local reversibility.

More recent operando FIB-SIMS work demonstrates how the same state-resolved principle can be extended from morphology to chemistry. Sharma et al. developed an operando FIB-SEM-SIMS configuration in which a solid-state Li cell remained electrically active during secondary-electron and SIMS imaging, and isotope tracing was used to follow changes in Li distribution under applied current [41]. This represents a higher level of evidence than repeated morphology alone because electrochemical state, spatially resolved chemical signal, and externally imposed current are linked within the same experiment. Nevertheless, interpretation still requires control of surface topography, sample bias, beam exposure, and the extent to which the analytical geometry perturbs normal cell operation.

5.2. Morphological Observations and Derived Geodesic Descriptors

To compare the geometrical consequences of damage, the image sequence was aligned, cropped, and segmented into NMC622 and Li_3PS_4 domains before geodesic distances were calculated [18]. The NMC622/Li_3PS_4 interface served as the starting marker and the segmented NMC phase as the admissible mask. Each value is the shortest connected distance through that two-dimensional mask to a point inside an NMC622 particle. The descriptor therefore translates observed morphology into a reproducible path-length distribution, but

it is not a general Li-ion pathway. Chemical-potential gradients, diffusivity, charge-transfer kinetics, electronic conduction, stress-dependent transport, and out-of-plane connections are absent from the calculation. Figure 5 summarizes the corresponding geodesic-distance maps and path-length distributions for the pristine, first-cycle, and constructed prolonged-cycling states.

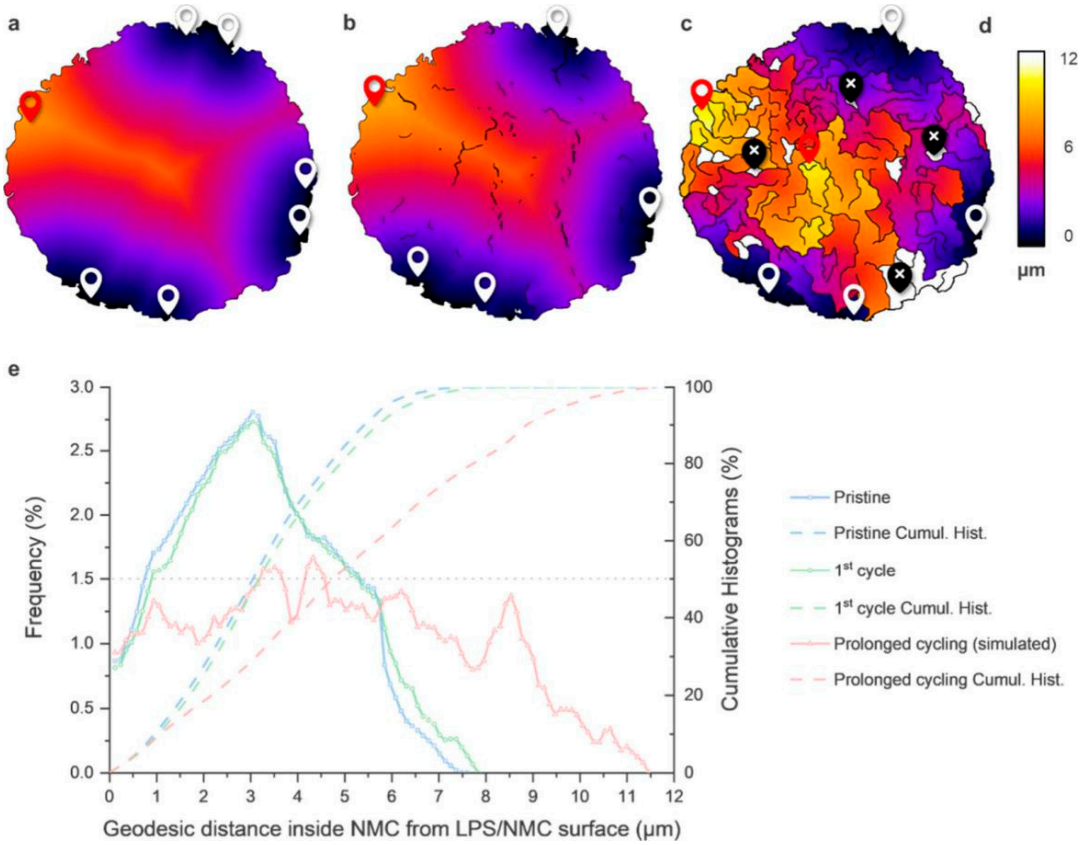


Figure 5. Cross-sectional geodesic descriptors derived from an NMC622/Li_3PS_4 electrode. (**a**) Geodesic-distance map for the pristine morphology; (**b**) geodesic-distance map after the first electrochemical cycle; (**c**) geodesic-distance map for the constructed prolonged-cycling damage scenario; (**d**) color scale used for the geodesic distance; and (**e**) frequency and cumulative distributions of the calculated path lengths for the pristine, first-cycle, and simulated prolonged-cycling states. Distances are calculated within the segmented two-dimensional NMC622 phase from the NMC622/Li_3PS_4 interface. The metric describes morphology-dependent geometry rather than Li flux, diffusivity, or conductivity. Adapted with permission from Ref. [18]. Copyright 2024 American Chemical Society.

The resulting geodesic distribution is a morphology-dependent descriptor of connected path length within the segmented two-dimensional NMC phase. Broadening or shifting of this distribution indicates that portions of the segmented particle are connected to the assigned NMC622/Li_3PS_4 interface through less direct geometrical routes. The descriptor should not be interpreted as Li-ion diffusivity or resistance because chemical-potential gradients, charge-transfer kinetics, electronic conduction, and out-of-plane connections are absent. Its value also depends on interface placement, phase segmentation, and treatment of partially closed cracks; threshold-sensitivity analysis is therefore required before small differences are interpreted physically.

5.3. How the Observation Window Perturbs the Experiment

The operando window is not a passive view into an unchanged electrode. The reported initial open-circuit voltage was approximately 1.9 V, compared with about 2.1 V

for a conventional cell, consistent with lower effective stack pressure and a larger ohmic contribution in the modified geometry [18]. A separate ion-beam test produced a potential fluctuation of about 200 mV, after which state-resolved imaging relied on low-dose SEM rather than continuous FIB probing. Dose, face cleaning, vacuum time, contamination, and contrast evolution therefore belong to the experimental record. Cleaning can restore visibility but may also remove material, smooth a partially closed crack, or change the surface being compared.

Neither voltage difference isolates the mechanical effect of the trench itself. Milling creates a free surface, reduces confinement on one side, and may permit strain relaxation precisely where particle breathing, fracture opening, and interface decohesion are being examined. The most direct control would compare window-adjacent behavior with untrenched or interior regions under similar electrochemical loading. Without that comparison, the observation applies to the prepared window under the stated pressure and cell configuration. Independent tomography and pressure-recovery studies support the broader electrochemical relevance of contact loss, but they do not substitute for a control of the local window geometry [42].

A practical control hierarchy can separate these perturbations more systematically. First, the electrochemical response of the modified cell should be compared with that of an otherwise equivalent unmodified cell before and after window preparation, using quantities such as OCV, polarization, impedance, or capacity. Second, window-adjacent behavior should be compared with an untrenched or interior region under matched stack pressure and thermal history. Third, beam effects should be assessed through beam-off controls or dose-series tests, with the electrical response monitored before and after exposure. For cryogenic or protected-transfer workflows, transfer time, temperature, atmosphere, and vacuum history should be documented and, where feasible, compared with matched room-temperature or differently protected specimens. Finally, microscopy-derived changes should be cross-checked against independent electrochemical or larger-field measurements when the claim extends beyond the local observation window.

The sampled field contains few particles and one cross-section, so particle size, orientation, contact quality, porosity, and electrode position can influence the apparent response. The geodesic metric remains two-dimensional and cannot capture out-of-plane bypasses. The supported conclusion is therefore local: near the prepared window, specific fractures and interface gaps opened at defined electrochemical states and some narrowed during lithiation. Linking those changes to transport requires independent electrochemical or modelling evidence, while estimating their prevalence requires additional particles, windows, or three-dimensional measurements.

6. Choosing the Workflow and Reporting the Evidence

6.1. Matching the FIB-Defined Geometry to the Missing Analytical Dimension

Workflow selection should begin by identifying the missing analytical dimension in the scientific question rather than by selecting the most elaborate available instrument. If local chemistry must be assigned to electrode depth or a prelocated buried feature, a targeted surface is sufficient. If the claim depends on persistence or adjacency outside one plane, a registered depth sequence is required. If the timing or partial reversibility of structural change is unresolved, the same cross-section must be revisited at defined electrochemical states. The preferred workflow is therefore the least invasive FIB-defined geometry that resolves the relevant ambiguity while leaving the subsequent measurement-to-claim chain testable.

Table 1 also shows that more elaborate acquisition does not necessarily produce stronger evidence. A large registered volume remains chemically ambiguous if matrix

effects or alignment errors are unconstrained, whereas a single targeted plane can answer the question decisively when only the location of a buried feature is unknown. Operando imaging supplies state order but also changes local pressure, resistance, and mechanical confinement.

6.2. Building the Measurement-to-Claim Chain

Across all four workflows, evidence strength depends not only on acquisition quality but also on the transformations between the acquired signal and the final interpretation. The recommended reporting sequence is therefore: FIB-defined geometry → direct signal → transformation → derived quantity → validation → physical claim. Each step should remain traceable to the preceding one, and the uncertainty introduced during processing should be evaluated relative to the spatial or temporal relation being interpreted.

This hierarchy prevents different evidence levels from being conflated. Relative SIMS intensity should not be presented as absolute concentration without appropriate calibration; apparent continuity in a registered three-dimensional rendering should not automatically be interpreted as a transport pathway; and state-resolved morphological evolution does not by itself establish a kinetic or electrochemical mechanism. Stronger claims require either demonstrated robustness of the derived quantity or complementary evidence that probes the corresponding physical process independently. Table 2 summarizes terminology that preserves these evidentiary distinctions at the level of the reported quantity and claim.

Table 2. Recommended terminology and evidentiary limits for FIB-supported correlative battery characterization.

Observed/Derived Quantity	Recommended Wording	Supported Interpretation	Avoid Unless Independently Validated
EDS/SIMS intensity	Relative signal intensity/distribution	Relative spatial signal under stated conditions	Concentration, stoichiometry, local SOC
Registered multimodal domains	Spatial association/co-location within registration uncertainty	Association of signals within stated resolution/error	Chemical causality or exact phase boundary
Segmented connectivity	Image-derived geometrical connectivity	Connectivity of the segmented domain in the analyzed volume	Ionic/electronic transport pathway
Geodesic/path-length metric	Geometry-based path-length descriptor	Morphology-dependent path geometry	Diffusivity, resistance, or flux
Repeated 2D cross-section	State-resolved local structural evolution	Event order and local reversibility in the observed plane	3D prevalence or electrode-wide degradation mechanism
Operando/state-resolved in-cell/post-mortem	Use according to acquisition timing	Acquisition timing relative to active device operation	Interchangeable use of these terms

Complementary evidence should be selected according to the physical claim being tested rather than added indiscriminately. For electrochemical-state assignment, current, voltage, passed capacity, and independently estimated state of charge can establish whether spatial observations correspond to comparable operating states [43]. Robust SOC estimation across changing temperature or operating conditions can therefore provide an orthogonal state label when microscopy is performed on cells subjected to non-identical histories. For dynamic or kinetic consequences, impedance spectroscopy, current-interruption methods, GITT/PITT, or broadband perturbation measurements can test whether an observed struc-

tural or interfacial change coincides with a measurable change in electrochemical response. Fast multisine-based characterization is one example because impedance and nonlinear response can be obtained on a timescale compatible with state-dependent degradation assessment [44].

A still stronger mechanistic claim requires correspondence across more than one evidence level. A reconstructed contact loss, for example, may be associated with increased resistance if the same electrochemical transition is accompanied by an independently measured impedance change; a Li-sensitive spatial gradient becomes more transport-relevant when isotope tracing or controlled electrochemical forcing establishes its evolution with current [41]; and an image-derived pathway becomes physically meaningful only when transport modelling or an independent kinetic measurement is consistent with the geometrical prediction. These combinations do not make microscopy a direct transport measurement; rather, they establish an evidence chain in which geometry, state, function, and physical interpretation remain separately testable.

6.3. Reporting Uncertainty and Minimum Validation

The purpose of quantitative reporting is not to impose universal acceptance thresholds across instruments or battery chemistries. Instead, each uncertainty should be compared with the scale of the feature, displacement, enrichment zone, or state-dependent change being interpreted. A relocation error of several hundred nanometres may be negligible for a micrometre-scale particle but decisive for assigning chemistry to a nanoscale interface. Where possible, uncertainty should therefore be reported both as an absolute value and relative to the characteristic scale of the feature or displacement being interpreted. For processing-derived descriptors, the corresponding result should also be reported over a justified range of registration or segmentation parameters rather than for a single selected parameter set.

Table 1 converts these sources of uncertainty into workflow-specific minimum reporting requirements; where numerical uncertainty can be estimated, values should be reported rather than described only qualitatively.

For targeted surfaces, the critical record includes the selection rule, orientation or tomographic landmarks, electrochemical state, transfer environment, protective deposition, milling conditions, final polish, and effective target-plane uncertainty. Reactive lithium, sulfide, polymer-containing, or liquid-containing specimens may require cryogenic or protected transfer, but preservation should be validated against the signal used in the final claim [19,20,25]. For serial reconstructions, measured slice spacing, acquisition order, field overlap, voxel dimensions, registration residuals, excluded regions, and segmentation sensitivity should be reported. Operando studies additionally require cell geometry, stack loading, trench dimensions, beam history, imaging states, and comparison with conventional or untrenched configurations. Captions should identify data as acquired, registered, reconstructed, segmented, calculated, or simulated; relative intensity should not be presented as concentration, and geometry-based connectivity or path length should not be labelled as measured transport.

Relocation, registration, and segmentation uncertainty is rarely propagated into the final elemental-association, connectivity, or path descriptor. Multimodal fiducials, reported residuals, low-damage preparation, and parameter-sensitivity tests are needed to show whether the conclusion survives plausible analytical variation. Figures that combine raw images, normalized maps, registered volumes, calculated descriptors, and simulated states should label each category. Representative source planes, registration residuals, and segmentation checks should accompany final renderings in the supporting information.

Uncertainty propagation should be tied to the derived quantity rather than treated only as an acquisition parameter. For cross-modal elemental co-location, one practical approach is to translate or rotate one modality over the measured registration-residual range and report the resulting variation in overlap fraction, nearest-interface distance, or other association metrics. For serial reconstructions, uncertainty in slice spacing or removed depth can be propagated by rebuilding the volume over the calibrated spacing range and reporting the variation in volume-, interface-, or path-based descriptors. Segmentation-derived quantities such as connected fraction, crack density, interface area, or geodesic distance should likewise be recalculated over a justified threshold or segmentation ensemble rather than reported from a single mask. Where several uncertainties act simultaneously, bootstrap or Monte Carlo resampling of the measured parameter ranges can provide an uncertainty interval for the final descriptor. The appropriate output is therefore not only a nominal value, but the range over which the physical conclusion remains unchanged. For example, an apparent interfacial enrichment is robust only if the association persists after registration perturbations comparable to the measured residual, whereas a reported crack-density change should exceed the variation produced by plausible segmentation thresholds. Not all uncertainties are geometric or segmentation-based. Matrix-dependent chemical signals should, where feasible, be bounded using matrix-matched standards, within-phase replicate measurements, or other appropriate calibration controls, whereas beam-induced modification and redeposition can be evaluated through dose-series, beam-off, and pre-/post-exposure comparisons. The resulting variation in signal intensity, apparent interface position, or morphology should be carried into any co-location, enrichment, crack-density, or related descriptor that depends on the affected data.

6.4. Representativeness and Practical Priorities

High-resolution FIB volumes are often too small and too selectively chosen to represent an electrode. Repeated regions, predefined sampling rules, validated automated segmentation, and multiscale correlation can connect local detail to population-level statistics [7,34,36]. Correlative transfer to TEM, STEM, or atom-probe tomography can add atomic-scale information at a selected interface, but it does not remove the need to establish how that interface was chosen or how representative it is [27].

The required number of regions cannot be defined by a universal minimum because it depends on the claim and the spatial variance of the electrode. A deliberately targeted ROI can establish the existence of a local phenomenon under the reported conditions, but it cannot estimate prevalence. Reproducibility claims require the same observation to be repeated in independently selected regions and, where possible, independent cells. Population-level quantities require random, systematic, or stratified sampling across the relevant electrode coordinates, with the numbers of regions (n_{ROI}) and independent cells (n_{cell}) reported separately. Sample size should be determined from pilot variability and the desired confidence or precision of the final descriptor rather than from an arbitrary fixed number. For rare-feature studies, targeted ROIs may be used to interrogate mechanism, but a separate unbiased sampling set is needed to estimate prevalence. Bootstrap resampling or convergence of the mean, median, or prevalence estimate with increasing n provides a practical test of whether additional regions materially change the conclusion.

Future FIB studies should report three linked elements: the FIB-defined analytical geometry, the signal acquired within that geometry, and every transformation applied before physical interpretation. A targeted geometry can establish a local structural-chemical association; serial reconstruction can establish cross-depth persistence and adjacency when registration and segmentation are quantified; and a revisited observation window can establish event order when window-induced perturbation is controlled. Claims concerning

ionic transport, reaction kinetics, or degradation mechanisms require complementary evidence that probes those processes independently.

7. Conclusions

FIB-defined analytical geometries are most useful when they recover information that would otherwise be lost: position, depth/volume, or electrochemical state/time. Their evidentiary value, however, depends on maintaining traceability from the acquired signal through registration, reconstruction, segmentation, or other transformations to the final physical claim. Relative elemental intensity, geometrical connectivity, and state-resolved morphology should not be conflated with concentration, transport, or three-dimensional mechanism without independent validation. Equally importantly, analytical credibility and population representativeness are separate requirements. A deliberately targeted feature can establish a local phenomenon, but electrode-wide prevalence requires predefined sampling across multiple regions and independent specimens. Future FIB-supported battery studies should therefore report both the uncertainty of the analytical chain and the sampling basis on which broader conclusions are made.

Author Contributions: Conceptualization, J.J. and Z.D.; literature investigation, J.J., Y.L. (Yong Li), K.D. and Y.L. (Yuchen Li); visualization, J.J. and K.D.; writing—original draft preparation, J.J.; writing—review and editing, J.J., Y.L. (Yong Li), K.D., Y.L. (Yuchen Li), Z.D. and M.A.; supervision, Z.D. All authors have read and agreed to the published version of the manuscript.

Funding: This research received no external funding.

Data Availability Statement: No new data were created or analyzed in this study. Data sharing is not applicable to this article.

Conflicts of Interest: The authors declare no conflicts of interest.

References

1. Janek, J.; Zeier, W.G. A Solid Future for Battery Development. *Nat. Energy* **2016**, *1*, 16141. [CrossRef]
2. Manthiram, A. A Reflection on Lithium-Ion Battery Cathode Chemistry. *Nat. Commun.* **2020**, *11*, 1550. [CrossRef]
3. Lewis, J.A.; Quintero Cortes, F.J.; Liu, Y.; Miers, J.C.; Verma, A.; Vishnugopi, B.S.; Tippens, J.; Prakash, D.; Marchese, T.S.; Han, S.Y.; et al. Linking Void and Interphase Evolution to Electrochemistry in Solid-State Batteries Using Operando X-Ray Tomography. *Nat. Mater.* **2021**, *20*, 503–510. [CrossRef]
4. Dixit, M.B.; Singh, N.; Horwath, J.P.; Shevchenko, P.D.; Jones, M.; Stach, E.A.; Arthur, T.S.; Hatzell, K.B. In Situ Investigation of Chemomechanical Effects in Thiophosphate Solid Electrolytes. *Matter* **2020**, *3*, 2138–2159. [CrossRef]
5. Chang, W.; May, R.; Wang, M.; Thorsteinsson, G.; Sakamoto, J.; Marbella, L.; Steingart, D. Evolving Contact Mechanics and Microstructure Formation Dynamics of the Lithium Metal-$Li_7La_3Zr_2O_{12}$ Interface. *Nat. Commun.* **2021**, *12*, 6369. [CrossRef]
6. Pietsch, P.; Wood, V. X-Ray Tomography for Lithium Ion Battery Research: A Practical Guide. *Annu. Rev. Mater. Res.* **2017**, *47*, 451–479. [CrossRef]
7. Scharf, J.; Chouchane, M.; Finegan, D.P.; Lu, B.; Redquest, C.; Kim, M.-C.; Yao, W.; Franco, A.A.; Gostovic, D.; Liu, Z.; et al. Bridging Nanoand Microscale X-Ray Tomography for Battery Research by Leveraging Artificial Intelligence. *Nat. Nanotechnol.* **2022**, *17*, 446–459. [CrossRef]
8. Moroni, R.; Börner, M.; Zielke, L.; Schroeder, M.; Nowak, S.; Winter, M.; Manke, I.; Zengerle, R.; Thiele, S. Multi-Scale Correlative Tomography of a Li-Ion Battery Composite Cathode. *Sci. Rep.* **2016**, *6*, 30109. [CrossRef]
9. Ender, M.; Joos, J.; Carraro, T.; Ivers-Tiffée, E. Three-Dimensional Reconstruction of a Composite Cathode for Lithium-Ion Cells. *Electrochem. Commun.* **2011**, *13*, 166–168. [CrossRef]
10. Sui, T.; Song, B.; Dluhos, J.; Lu, L.; Korsunsky, A.M. Nanoscale Chemical Mapping of Li-Ion Battery Cathode Material by FIB-SEM and TOF-SIMS Multi-Modal Microscopy. *Nano Energy* **2015**, *17*, 254–260. [CrossRef]
11. Pillatsch, L.; Östlund, F.; Michler, J. FIBSIMS: A Review of Secondary Ion Mass Spectrometry for Analytical Dual Beam Focused Ion Beam Instruments. *Prog. Cryst. Growth Charact. Mater.* **2019**, *65*, 1–19. [CrossRef]
12. Lombardo, T.; Walther, F.; Kern, C.; Moryson, Y.; Weintraut, T.; Henss, A.; Rohnke, M. ToF-SIMS in Battery Research: Advantages, Limitations, and Best Practices. *J. Vac. Sci. Technol. A* **2023**, *41*, 053207. [CrossRef]

13. Liu, Z.; Bai, S.; Burke, S.; Burrow, J.N.; Geurts, R.; Huang, C.-J.; Jiao, C.; Lee, H.-B.; Meng, Y.S.; Novák, L.; et al. FIB-SEM: Emerging Multimodal/Multiscale Characterization Techniques for Advanced Battery Development. *Chem. Rev.* **2025**, *125*, 5228–5281. [CrossRef]
14. Bai, S.; Liu, Z.; Cheng, D.; Lu, B.; Zaluzec, N.J.; Raghavendran, G.; Wang, S.; Marchese, T.S.; van Leer, B.; Li, L.; et al. Guidelines for Correlative Imaging and Analysis of Reactive Alkali Metal Battery Materials. *Joule* **2026**, *10*, 102311. [CrossRef]
15. Delfino, P.M.; Bofanova, M.; De Vito, E.; Dupré, N.; Lamblin, G.; Porcher, W.; Wirtz, T.; Audinot, J.-N. Lift-Out Specimen Preparation and Multiscale Correlative Investigation of Li-Ion Battery Electrodes Using Focused Ion Beam-Secondary Ion Mass Spectrometry Platforms. *ACS Appl. Mater. Interfaces* **2024**, *16*, 57141–57150. [CrossRef]
16. Cressa, L.; Fell, J.; Pauly, C.; Hoang, Q.H.; Mücklich, F.; Herrmann, H.-G.; Wirtz, T.; Eswara, S. A FIB-SEM-Based Correlative Methodology for X-Ray Nanotomography and Secondary Ion Mass Spectrometry: An Application Example in Lithium Batteries Research. *Microsc. Microanal.* **2022**, *28*, 1890–1895. [CrossRef]
17. Sun, Y.; Hughes, G.M.; Bu, J.; Liu, J.; Grovenor, C.R.M.; Grant, P.S. Visualizing the Li Distribution in an All-Solid-State Battery Composite Electrode Using Combined Plasma Focused-Ion Beam Microscopy and Secondary-Ion Mass Spectroscopy. *Micron* **2025**, *190*, 103746. [CrossRef]
18. Perrenot, P.; Bayle-Guillemaud, P.; Jouneau, P.-H.; Boulineau, A.; Villevieille, C. Operando Focused Ion Beam-Scanning Electron Microscope (FIB-SEM) Revealing Microstructural and Morphological Evolution in a Solid-State Battery. *ACS Energy Lett.* **2024**, *9*, 3835–3840. [CrossRef]
19. Lee, J.Z.; Wynn, T.A.; Schroeder, M.A.; Alvarado, J.; Wang, X.; Xu, K.; Meng, Y.S. Cryogenic Focused Ion Beam Characterization of Lithium Metal Anodes. *ACS Energy Lett.* **2019**, *4*, 489–493. [CrossRef]
20. Zachman, M.J.; Tu, Z.; Choudhury, S.; Archer, L.A.; Kourkoutis, L.F. Nanoscale Elemental Mapping of Intact Solid-Liquid Interfaces and Reactive Materials in Energy Devices Enabled by Cryo-FIB/SEM. *ACS Energy Lett.* **2020**, *5*, 1224–1232. [CrossRef]
21. Bessette, S.; Paolella, A.; Kim, C.; Zhu, W.; Hovington, P.; Gauvin, R.; Zaghib, K. Nanoscale Lithium Quantification in $Li_xNi_yCo_wMn_zO_2$ as Cathode for Rechargeable Batteries. *Sci. Rep.* **2018**, *8*, 17575. [CrossRef]
22. Masuda, H.; Ishida, N.; Ogata, Y.; Ito, D.; Fujita, D. In Situ Visualization of Li Concentration in All-Solid-State Lithium-Ion Batteries Using Time-of-Flight Secondary Ion Mass Spectrometry. *J. Power Sources* **2018**, *400*, 527–532. [CrossRef]
23. Cressa, L.; Sun, Y.; Andersen, D.; Gerard, M.; De Castro, O.; Kopljar, D.; Nojabaee, M.; Friedrich, K.A.; Schmitz, G.; Wirtz, T.; et al. Toward Operando Structural, Chemical, and Electrochemical Analyses of Solid-State Batteries Using Correlative Secondary Ion Mass Spectrometry Imaging. *Anal. Chem.* **2023**, *95*, 9932–9939. [CrossRef]
24. Li, Y.; Li, Y.; Pei, A.; Yan, K.; Sun, Y.; Wu, C.-L.; Joubert, L.-M.; Chin, R.; Koh, A.L.; Yu, Y.; et al. Atomic Structure of Sensitive Battery Materials and Interfaces Revealed by Cryo-Electron Microscopy. *Science* **2017**, *358*, 506–510. [CrossRef]
25. Zachman, M.J.; Tu, Z.; Choudhury, S.; Archer, L.A.; Kourkoutis, L.F. Cryo-STEM Mapping of Solid-Liquid Interfaces and Dendrites in Lithium-Metal Batteries. *Nature* **2018**, *560*, 345–349. [CrossRef]
26. Chae, B.-G.; Park, S.Y.; Song, J.H.; Lee, E.; Jeon, W.S. Evolution and Expansion of Li Concentration Gradient during Charge-Discharge Cycling. *Nat. Commun.* **2021**, *12*, 3814. [CrossRef]
27. Pantenburg, I.; Cronau, M.; Boll, T.; Duncker, A.; Roling, B. Challenging Prevalent Solid Electrolyte Interphase (SEI) Models: An Atom Probe Tomography Study on a Commercial Graphite Electrode. *ACS Nano* **2023**, *17*, 21531–21538. [CrossRef]
28. Zielke, L.; Hutzenlaub, T.; Wheeler, D.R.; Manke, I.; Arlt, T.; Paust, N.; Zengerle, R.; Thiele, S. A Combination of X-Ray Tomography and Carbon Binder Modeling: Reconstructing the Three Phases of $LiCoO_2$ Li-Ion Battery Cathodes. *Adv. Energy Mater.* **2014**, *4*, 1301617. [CrossRef]
29. Hutzenlaub, T.; Asthana, A.; Becker, J.; Wheeler, D.R.; Zengerle, R.; Thiele, S. FIB/SEM-Based Calculation of Tortuosity in a Porous $LiCoO_2$ Cathode for a Li-Ion Battery. *Electrochem. Commun.* **2013**, *27*, 77–80. [CrossRef]
30. Hutzenlaub, T.; Thiele, S.; Paust, N.; Spotnitz, R.; Zengerle, R.; Walchshofer, C. Three-Dimensional Electrochemical Li-Ion Battery Modelling Featuring a Focused Ion-Beam/Scanning Electron Microscopy Based Three-Phase Reconstruction of a $LiCoO_2$ Cathode. *Electrochim. Acta* **2014**, *115*, 131–139. [CrossRef]
31. Daemi, S.R.; Tan, C.; Volkenandt, T.; Cooper, S.J.; Palacios-Padros, A.; Cookson, J.; Brett, D.J.L.; Shearing, P.R. Visualizing the Carbon Binder Phase of Battery Electrodes in Three Dimensions. *ACS Appl. Energy Mater.* **2018**, *1*, 3702–3710. [CrossRef]
32. Almar, L.; Joos, J.; Weber, A.; Ivers-Tiffée, E. Microstructural Feature Analysis of Commercial Li-Ion Battery Cathodes by Focused Ion Beam Tomography. *J. Power Sources* **2019**, *427*, 1–14. [CrossRef]
33. Liu, H.; Foster, J.M.; Gully, A.; Krachkovskiy, S.; Jiang, M.; Wu, Y.; Yang, X.; Protas, B.; Goward, G.R.; Botton, G.A. Three-Dimensional Investigation of Cycling-Induced Microstructural Changes in Lithium-Ion Battery Cathodes Using Focused Ion Beam/Scanning Electron Microscopy. *J. Power Sources* **2016**, *306*, 300–308. [CrossRef]
34. Müller, S.; Sauter, C.; Shunmugasundaram, R.; Wenzler, N.; De Andrade, V.; De Carlo, F.; Konukoglu, E.; Wood, V. Deep Learning-Based Segmentation of Lithium-Ion Battery Microstructures Enhanced by Artificially Generated Electrodes. *Nat. Commun.* **2021**, *12*, 6205. [CrossRef]

35. Lu, X.; Bertei, A.; Finegan, D.P.; Tan, C.; Daemi, S.R.; Weaving, J.S.; O'Regan, K.B.; Heenan, T.M.M.; Hinds, G.; Kendrick, E.; et al. 3D Microstructure Design of Lithium-Ion Battery Electrodes Assisted by X-Ray Nano-Computed Tomography and Modelling. *Nat. Commun.* **2020**, *11*, 2079. [CrossRef]
36. Jiang, Z.; Li, J.; Yang, Y.; Mu, L.; Wei, C.; Yu, X.; Pianetta, P.; Zhao, K.; Cloetens, P.; Lin, F.; et al. Machine-Learning-Revealed Statistics of the Particle-Carbon/Binder Detachment in Lithium-Ion Battery Cathodes. *Nat. Commun.* **2020**, *11*, 2310. [CrossRef]
37. Hovington, P.; Timoshevskii, V.; Burgess, S.; Demers, H.; Statham, P.; Gauvin, R.; Zaghib, K. Can We Detect Li K X-Ray in Lithium Compounds Using Energy Dispersive Spectroscopy? *Scanning* **2016**, *38*, 571–578. [CrossRef]
38. Burnett, T.L.; Kelley, R.; Winiarski, B.; Contreras, L.; Daly, M.; Gholinia, A.; Burke, M.G.; Withers, P.J. Large Volume Serial Section Tomography by Xe Plasma FIB Dual Beam Microscopy. *Ultramicroscopy* **2016**, *161*, 119–129. [CrossRef]
39. Wu, X.; Billaud, J.; Jerjen, I.; Marone, F.; Ishihara, Y.; Adachi, M.; Adachi, Y.; Villevieille, C.; Kato, Y. Operando Visualization of Morphological Dynamics in All-Solid-State Batteries. *Adv. Energy Mater.* **2019**, *9*, 1901547. [CrossRef]
40. Huang, C.-J.; Oh, J.A.S.; Vicencio, M.; Hu, T.; Yang, H.; Burrow, J.N.; Song, Y.-F.; Yin, G.-C.; Shevchenko, P.; Wiaderek, K.M.; et al. X-Ray Micro-Computed Tomography for Structural Analysis of All-Solid-State Battery at Pouch Cell Level. *ACS Energy Lett.* **2025**, *10*, 3459–3470. [CrossRef]
41. Sharma, S.; Santiago, A.; Martinez-Ibañez, M.; Gerard, M.; Suresh Kumar, A.; De Castro, O.; Wirtz, T.; Eswara, S. Operando Visualization of Li Distribution in Solid-State Batteries Using Focused Ion Beam-Secondary Ion Mass Spectrometry Imaging. *Electrochim. Acta* **2025**, *536*, 146728. [CrossRef]
42. Shi, T.; Zhang, Y.-Q.; Tu, Q.; Wang, Y.; Scott, M.C.; Ceder, G. Characterization of Mechanical Degradation in an All-Solid-State Battery Cathode. *J. Mater. Chem. A* **2020**, *8*, 17399–17404. [CrossRef]
43. Fan, C.; Liu, Y.; Liu, K.; Li, M.; Turgun, Y.; Peng, Q. Two-Stage Prediction–Correction with Residual Compensation: A Framework for Robust State of Charge Estimation under Cross-Temperature Conditions. *J. Energy Storage* **2026**, *175*, 123275. [CrossRef]
44. Fan, C.; Zhang, K.; Peng, Q.; Tian, J.; Liu, K.; Chung, C.Y. Fast Characterization of Lithium-Ion Battery Impedance and Nonlinearity Using Optimized Multisine Perturbation Signal. *IEEE Trans. Ind. Electron.* **2025**, *72*, 11395–11405. [CrossRef]

Disclaimer/Publisher's Note: The statements, opinions and data contained in all publications are solely those of the individual author(s) and contributor(s) and not of MDPI and/or the editor(s). MDPI and/or the editor(s) disclaim responsibility for any injury to people or property resulting from any ideas, methods, instructions or products referred to in the content.